MNRAS 000, 1–6 (20242024) Preprint 6 November 2024 Compiled using MNRAS LATEX style file v3.3

Dazzle: Oversampled Image Reconstruction and Difference-Imaging Photometry for the Nancy Grace Roman Space Telescope.

Michael D. Albrow[1]★
[1]School of Physical and Chemical Sciences, University of Canterbury, Private Bag 4800, Christchurch, New Zealand

Accepted XXX. Received YYY; in original form ZZZ

ABSTRACT

This is a simple template for authors to write new MNRAS papers. The abstract should briefly describe the aims, methods, and main results of the paper. It should be a single paragraph not more than 250 words (200 words for Letters). No references should appear in the abstract.

Key words: keyword1 – keyword2 – keyword3

1 INTRODUCTION

The Nancy Grace Roman Space Telescope (formerly WFIRST, the Wide-Field Infrared Survey Telescope, and hereafter Roman) is expected to launch into L2 orbit in 2027. The Galactic Bulge Time Domain Survey (GBTDS) is one of three of Roman's Core Community Surveys. Using Roman's Wide Field Instrument (WFI), it is expected to monitor approximately 2 deg^2 towards the Galactic Bulge at low galactic latitudes with a 15-minute cadence. The survey is expected to continue for 6 yearly seasons of ~ 70 days (Penny et al. 2019; Wilson et al. 2023).

Current plans are for a pipeline of direct PSF-fitting photometry using the methods of Anderson & King (2000) from catalogued stars positions that will be established periodically through the duration of the survey. We expect that the direct photometric pipeline will provide excellent-quality photometry for the majority of microlensing events with bright source stars. For faint and/or blended source stars, difference-image photometry is likely to provide better results.

Difference imaging photometry (Tomaney & Crotts 1996; Alard & Lupton 1998; Alard 2000) has become the standard for Earth-based time-series imaging observations of crowded fields, and is used extensively for microlensing surveys of the Galactic Bulge (Wozniak 2000; Bond et al. 2001; Albrow et al. 2009). A difference-imaging approach was also used for two notable HST time series campaigns, the WFPC2 observations of the core of 47 Tuc (GO-8267) in 1999 (Gilliland et al. 2000; Albrow et al. 2001; Bruntt et al. 2001) and the ACS observations of Baade's Window in 2004 known as the SWEEPS project (GO-10475) (Sahu et al. 2006).

Terrestrial time-series imaging of crowded stellar fields usually have the following properties. (i) The individual images, T_k, are spatially over-sampled, i.e. there are at least 2.5 pixels spanning the full-width at half maximum intensity of the point-spread function (PSF; the intensity function of the image of a star on the detector). (ii) The width of the PSF is dominated by (variable) atmospheric seeing conditions. Under these assumptions, we can define a difference image,

$$D_k = T_k - R * K_k - B_k, \quad (1)$$

where R is a reference image created from one or more individual images with the sharpest PSF, $*$ is the convolution operator, K_k is a kernel that maps the PSF of R to the PSF of T_k, and B_k is the differential background. K_k may be decomposed as a linear sum of analytic functions (Alard & Lupton 1998) or as discrete pixel grid (Bramich et al. 2013). Depending on the representation, K_k can account for subpixel offsets between R and T_k. The challenge in ground-based PSF difference-imaging photometry is to compute K_k that minimizes the residuals in D_k.

In contrast, time-series images from space-based observatories like Roman have a PSF that is constant in time, but the individual images are usually spatially under-sampled, and have varying offsets (dithers) from each other. Difference-imaging photometry of these data requires completely different methods than those employed for over-sampled images. In this paper we present algorithms and software for a difference-image photometry pipeline for the Roman GBTDS.

2 SIMULATED DATA

In the description of the methodology that follows, we use a set of simulated images from the forthcoming Galactic Bulge Time Domain Survey.

To simulate the images, we first used the code *SYNTHPOP*[1] (Klüter et al., in prep) to simulate a population of stars in the direction of the Galactic Bulge centred on coordinates $(l, b) = (0, -3\,\mathrm{deg})$. The specific model incorporated the Besançon galactic stellar population model (Robin et al. 2003), with the extinction map from Marshall et al. (2006) and the reddening law from O'Donnell (1994) (see also Cardelli et al. (1989)).

We then used this catalogue as input to the *RomanISIM*[2] code

★ E-mail: michael.albrow@canterbury.ac.nz

[1] https://github.com/synthpop-galaxy/synthpop
[2] https://github.com/spacetelescope/romanisim

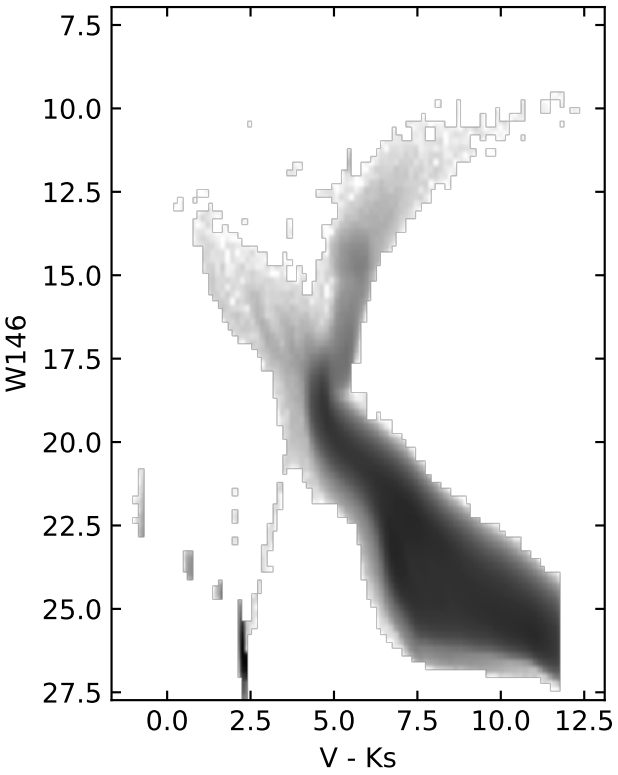

Figure 1. Hess diagram (shown in a log scale) of stars in the *SYNTHPOP* catalogue used as input to *RomanISIM*.

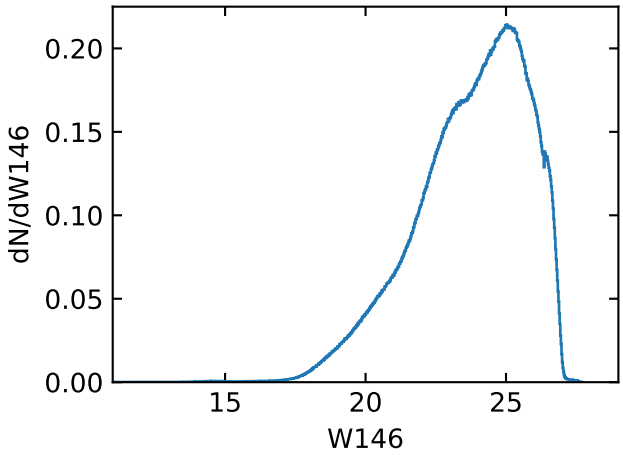

Figure 2. Luminosity function of stars in the *SYNTHPOP* catalogue used as input to *RomanISIM*.

to simulate Roman Level-2 images. We used the *WebbPSF*[3] (Perrin et al. 2014) option within *RomanISIM* for the stellar PSF's. The simulated images have an integration time of 145.92 s and saturation of ~ 2900 electron s^{-1}.

A short code, *RomanISim-simulate*[4], was used to control these steps. This code runs *SYNTHPOP* and converts the output to a format suitable for *RomanISIM*. It then runs *RomanISIM* to produce a set of images at a given observational cadence, introducing the stellar proper motions from *SYNTHPOP* and random dithers. The script can also be configured to inject point-source point-mass-lens microlensing events with given parameters onto sets of random stars of given magnitude ranges.

There are a total of 10.5 million stars in each of the simulated images. A Hess diagram and W146 luminosity function of the of the input stars are shown in Fig. 1 and Fig. 2 respectively.

3 DESCRIPTION OF THE ALGORITHM

3.1 Assumptions

We assume that our raw data consists of a set of images, $T_k(i, j)$, of a single region of the sky. The images are spatially under-sampled and dithered. For now, we assume that the dithering consists only of linear translations between images, with no differential rotation. The number of images, and the dithering pattern are sufficient to sample the sub-pixel space in a sense that will be described below. There is a known over-sampled effective PSF that can be evaluated for any image location.

3.2 Over-sampled image construction

Our aim here is to construct, $R(x, y)$, an over-sampled representation of the observed scene, after convolution by both the telescope optics and the pixel response function. That is, the image of a single star should have the shape of the effect point-spread function (ePSF) as defined by Anderson & King (2000).

As our reference grid, we adopt the pixel space of a single image, usually the first one, with indices defined at the pixel centres. The dithered offsets of each image from the reference are then determined, either from an astrometric solution found during previous processing (this will be the case for Roman) or some other means such as cross-correlation. Each pixel value in an image is a measurement of the over-sampled representation at its particular dither location.

It is convenient in what follows to split each dither offset from the reference grid for image k in the x direction into an integer part, Δx_k, and a sub-pixel part, δx_k, with a similar definition for offsets in the y direction. Thus each image,

$$T_{k,ij} = R(x_i + \Delta x_k + \delta x_k, y_j + \Delta y_k + \delta y_k) + \epsilon, \quad (2)$$

where ϵ means noise.

There are a number of potential representations that could be used to define the over-sampled image. For example

(i) A discrete array of pixels, defined at a higher spatial sampling than the original images. Interpolation between points on this grid could then be used to define the over-sampled image at any point.

(ii) A continuous two-dimensional analytic function, defined as a linear combination of basis functions that span the entire over-sampled image space. This would be a generalisation of the approach taken by Hogg & Casey (2024) for one-dimensional spectra.

(iii) A continuous spline representation, with knots defined on the boundaries of pixels in the reference grid.

(iv) A series of two-dimensional analytic functions, again defined as linear combinations of basis functions that individually span the space of single pixels in the reference grid.

We prefer to have an analytic representation, rather than (i), in order to avoid interpolation at later processing stages. After some

[3] https://github.com/spacetelescope/webbpsf
[4] https://github.com/MichaelDAlbrow/RomanISim-simulate

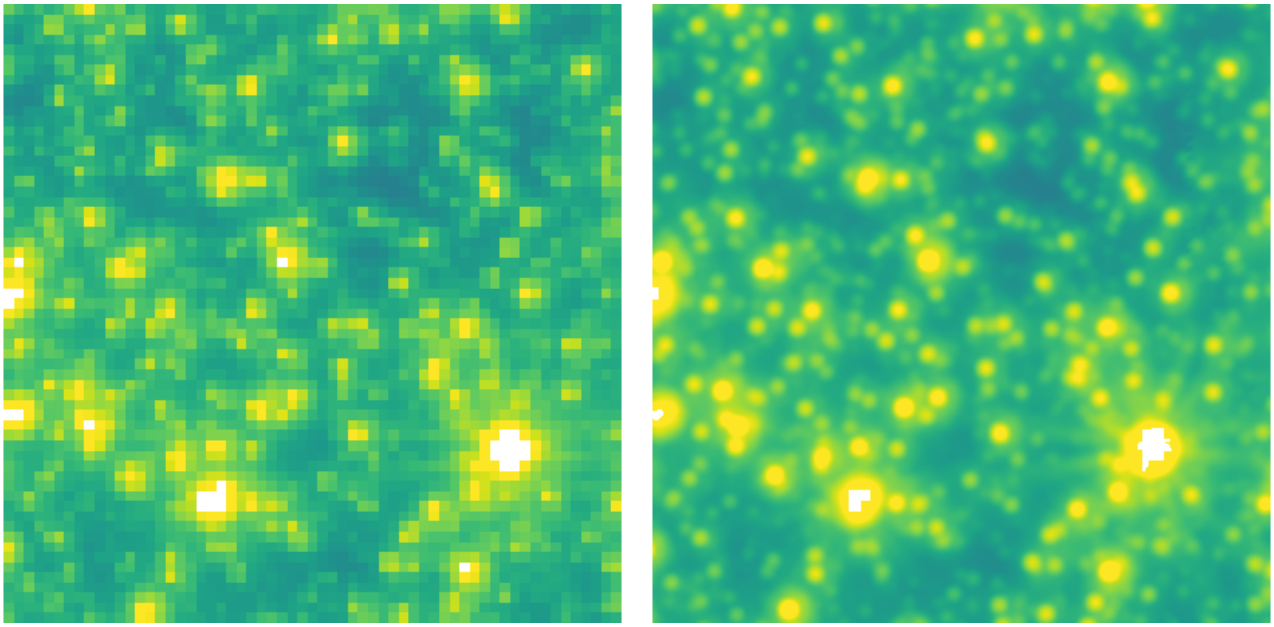

Figure 3. Sample 80 x 80 region of a simulated Roman image of the Galactic Bulge. Left panel: raw simulated image. Right panel: image at ten times the original sampling from a representation constructed from a stack of 192 randomly-dithered images. Panels have identical logarithmic intensity scaling and white pixels are saturated.

experimentation, we adopted the final option, (iv) above. Pragmatically, this is the solution that is computationally tractable (which is not the case for option (ii)) , and mathematically and computationally more simple than option (iii). This was also the approach taken by Gilliland et al. (2000). A further advantage is that the algorithm for over-sampled image generation described below is local for each pixel, and thus readily able to be parallelized.

We define our over-sampled representation of pixel (i, j) in the reference grid as

$$R_{ij}(x, y) = \sum_{l=1}^{N} \sum_{m=1}^{N} \theta_{ijlm} B_l(x - x_i) B_m(y - y_j), \tag{3}$$

where each $b_l(x)$ is a one-dimensional basis function of order N spanning $-0.5 < x \leq 0.5$. We choose our basis set to be the Legendre polynomials, $\mathcal{L}_l(x)$. Since $\mathcal{L}_l(x)$ are orthogonal over $-1 < x \leq 1$, we use $B_l(x) \equiv \mathcal{L}_l(2x)$.

A small disadvantage of this basis is that it does not require the representation to be continuous across pixel boundaries in the reference grid. To mitigate this, the over-sampled representation can be made very smooth by extending the basis functions into small overlap regions with neighbouring pixels, in which case $B_l(x) \equiv \mathcal{L}_l(2x/f)$ for extension factor f.

From experimentation with simulated Roman images, we found $N = 5$ with an extension factor $f = 1.2$, to work well for a smooth over-sampled representation and clean subsequent difference images.

We construct a design matrix, X, with elements

$$X[k, l + Nm] = B_l(\delta x_k) B_m(\delta y_k) \tag{4}$$

for images k with sub-pixel dithers $(\delta x_k, \delta y_k)$. If $f > 1$, extra rows are appended to X corresponding to the overlap pixel regions. This matrix is common for all image pixels.

Then, for each pixel (i, j) in the reference grid, we define a data vector, z_{ij}, with elements

$$z_{ij,k} = T_k(i + \Delta x_k, j + \Delta y_k) = T_{k,(i+\Delta x_k, j+\Delta y_k)} \tag{5}$$

for images k, again supplemented by rows for neighbouring pixels if $f > 1$. Note that we use the integer parts of the dithers in this expression.

Correspondingly, we define a data covariance matrix, C_{ij}, for each pixel, that is diagonal, with elements

$$C_{ij,kk} = \frac{1}{\sigma^2_{k,(i+\Delta x_k)(j+\Delta y_k)}}, \tag{6}$$

where $\sigma_{k,ij}$ is the uncertainty in $T_{k,ij}$.

For each pixel (i, j) in the reference grid, the coefficients, θ_{ijlm}, then have the standard linear algebraic solution,

$$\theta_{ijlm} \equiv a_{ij(l+Nm)} = (X^T C^{-1} X)^{-1} X^T C^{-1} z_{ij}, \tag{7}$$

that minimises

$$\chi^2 = \sum_k \frac{(T_{k,ij} - R_{kij})^2}{\sigma^2_{kij}}, \tag{8}$$

where R_{kij} means R evaluated at coordinates $(x_i + \Delta x_k + \delta x_k, y_j + \Delta y_k + \delta y_k)$.

For $N = 5$, there are 25 coefficients, θ_{ijlm}, for each reference grid pixel (i, j), so formally, 25 is the minimum number of images that can be combined to construct R, and only if the dithering pattern well-samples the sub-pixel space. In practice, with random dithers, we have found that 75 is a good minimum.

Maybe a note here about the K2 microlensing campaign.

In Fig. 3 we show an example region of a single simulated Roman image, together with an over-sampled representation constructed from 192 randomly dithered images.

3.3 Difference images

Once we have an over-sampled image representation, the process of creating difference images is straightforward. We define the difference image, D_k, corresponding to each original image T_{ij} as

$$D_{ij} = T_{kij} - R_{kij}. \tag{9}$$

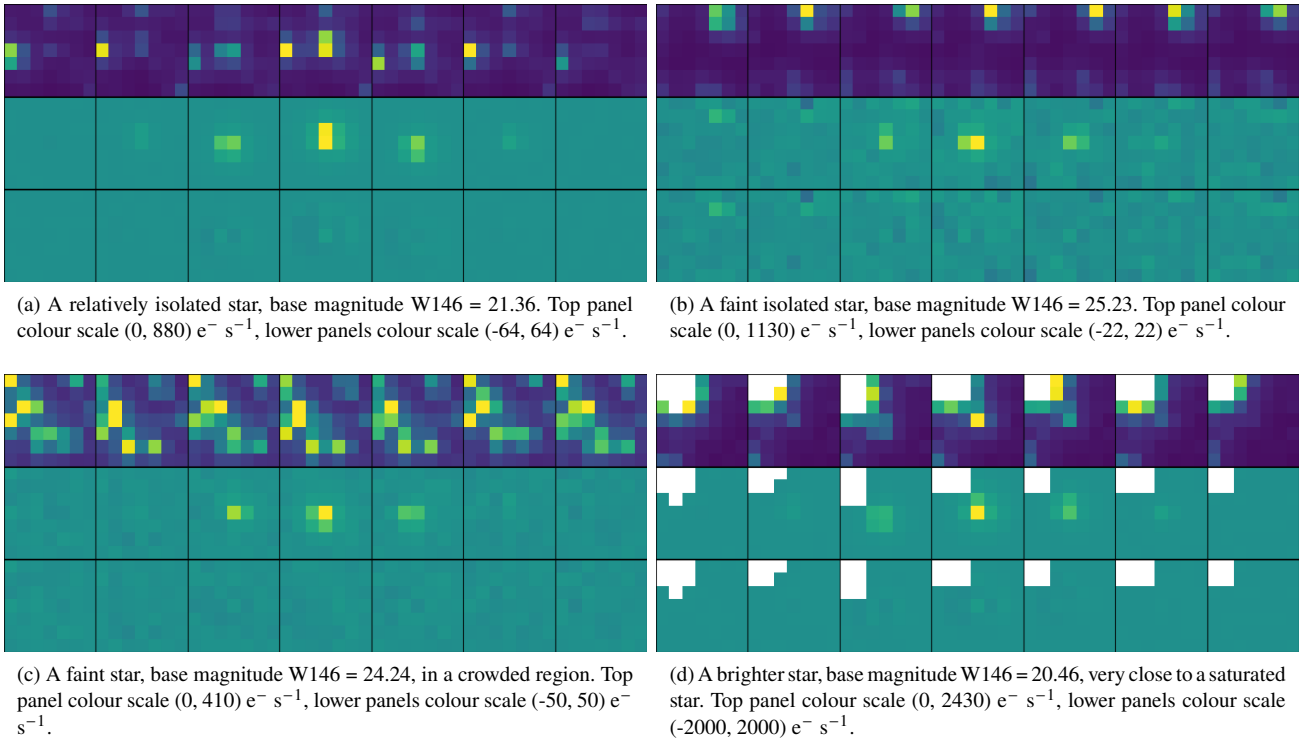

(a) A relatively isolated star, base magnitude W146 = 21.36. Top panel colour scale (0, 880) e^- s^{-1}, lower panels colour scale (-64, 64) e^- s^{-1}.

(b) A faint isolated star, base magnitude W146 = 25.23. Top panel colour scale (0, 1130) e^- s^{-1}, lower panels colour scale (-22, 22) e^- s^{-1}.

(c) A faint star, base magnitude W146 = 24.24, in a crowded region. Top panel colour scale (0, 410) e^- s^{-1}, lower panels colour scale (-50, 50) e^- s^{-1}.

(d) A brighter star, base magnitude W146 = 20.46, very close to a saturated star. Top panel colour scale (0, 2430) e^- s^{-1}, lower panels colour scale (-2000, 2000) e^- s^{-1}.

Figure 4. Four examples showing time series of sample 7 x 7 pixel stamp images centered on a star. In each case a PSPL microlensing light curve with parameters $u_0 = 0.1$, $t_0 = 2160$, $t_E = 400$ minutes has been injected directly into the stellar flux before image simulation. The top row of each panel shows the direct simulated images. The central rows are difference images, and the bottom rows are the same as the central rows, but after subtraction of the fitted PSF. Pixels that are saturated in the direct images are coloured white. Light curves from the complete sets of images are shown in Fig. 5. The images shown here are at times 0, 1950, 2100, 2160, 2220, 2370, 2865 min.

However, our procedures described above assume a temporally-constant underlying scene, with all pixel value measurements distributed about their true values in a Gaussian sense with known variances. Real images contain pixels that violate these assumptions. Discrepant pixel values can for example be due to cosmic rays, cosmetic detector defects, detector saturation, and variable stars.

To mitigate these effects, we perform the above steps in an iterative fashion, using the difference images to detect and mask bad pixel values on an image-by-image basis, before constructing a new over-sampled representation. In practice, the algorithm converges satisfactorily in three to five iterations.

3.4 Correction of offsets.

Assume that a single image, k, has a recorded dither position that is incorrect by a small amount. If (β_k, γ_k) is the offset that has to be applied to correct the dither position, then, assuming that the over-sampled representation is accurate, the corrected difference image will be

$$D'_{k,ij} = R(x_i + \Delta x_k + \delta x_k + \beta_k, y_j + \Delta y_k + \delta y_k + \gamma_k) - T_{k,ij} + \epsilon. \quad (10)$$

To first order,

$$\begin{aligned} R(x_i + \Delta x_k + \delta x_k + \beta_k, y_j + \Delta y_k + \delta y_k + \gamma_k) = R_{kij} \\ + \beta_k \left.\frac{\partial R}{\partial x}\right|_{(x_i+\Delta x_k+\delta x_k, y_j+\Delta y_k+\delta y_k)} \\ + \gamma_k \left.\frac{\partial R}{\partial y}\right|_{(x_i+\Delta x_k+\delta x_k, y_j+\Delta y_k+\delta y_k)}, \end{aligned} \quad (11)$$

so that

$$D'_{k,ij} = D_{k,ij} + \beta_k \frac{\partial R}{\partial x} + \gamma_k \frac{\partial R}{\partial y}, \quad (12)$$

with the (analytic) derivatives evaluated at the locations from Equation 11. Therefore, by minimizing

$$\chi^2 = \sum_k \frac{(D_{k,ij} + \beta_k \frac{\partial R}{\partial x} + \gamma_k \frac{\partial R}{\partial y})^2}{\sigma^2_{kij}}, \quad (13)$$

the offsets can be computed analytically as

$$[\beta_k, \gamma_k]^T = \mathbf{A}^{-1}\mathbf{b}, \quad (14)$$

where

$$\mathbf{A} = \begin{bmatrix} \sum_{ij} \frac{1}{\sigma^2_{kij}} \left(\frac{\partial R}{\partial x}\right)^2 & \sum_{ij} \frac{1}{\sigma^2_{kij}} \frac{\partial R}{\partial x} \frac{\partial R}{\partial y} \\ \sum_{ij} \frac{1}{\sigma^2_{kij}} \frac{\partial R}{\partial x} \frac{\partial R}{\partial y} & \sum_{ij} \frac{1}{\sigma^2_{kij}} \left(\frac{\partial R}{\partial y}\right)^2 \end{bmatrix}, \quad (15)$$

and

$$\mathbf{b} = -\left[\sum_{ij} \frac{D_{k,ij}}{\sigma^2_{kij}} \frac{\partial R}{\partial x}, \sum_{ij} \frac{D_{k,ij}}{\sigma^2_{kij}} \frac{\partial R}{\partial y}\right]^T. \quad (16)$$

The algorithm can be applied iteratively, making small adjustments to the individual image offsets at each iteration, before recomputing the oversampled representation. In practice this works well only for a small number of images with small dither errors, since it assumes that the initial over-sampled representation and its gradient are approximately correct.

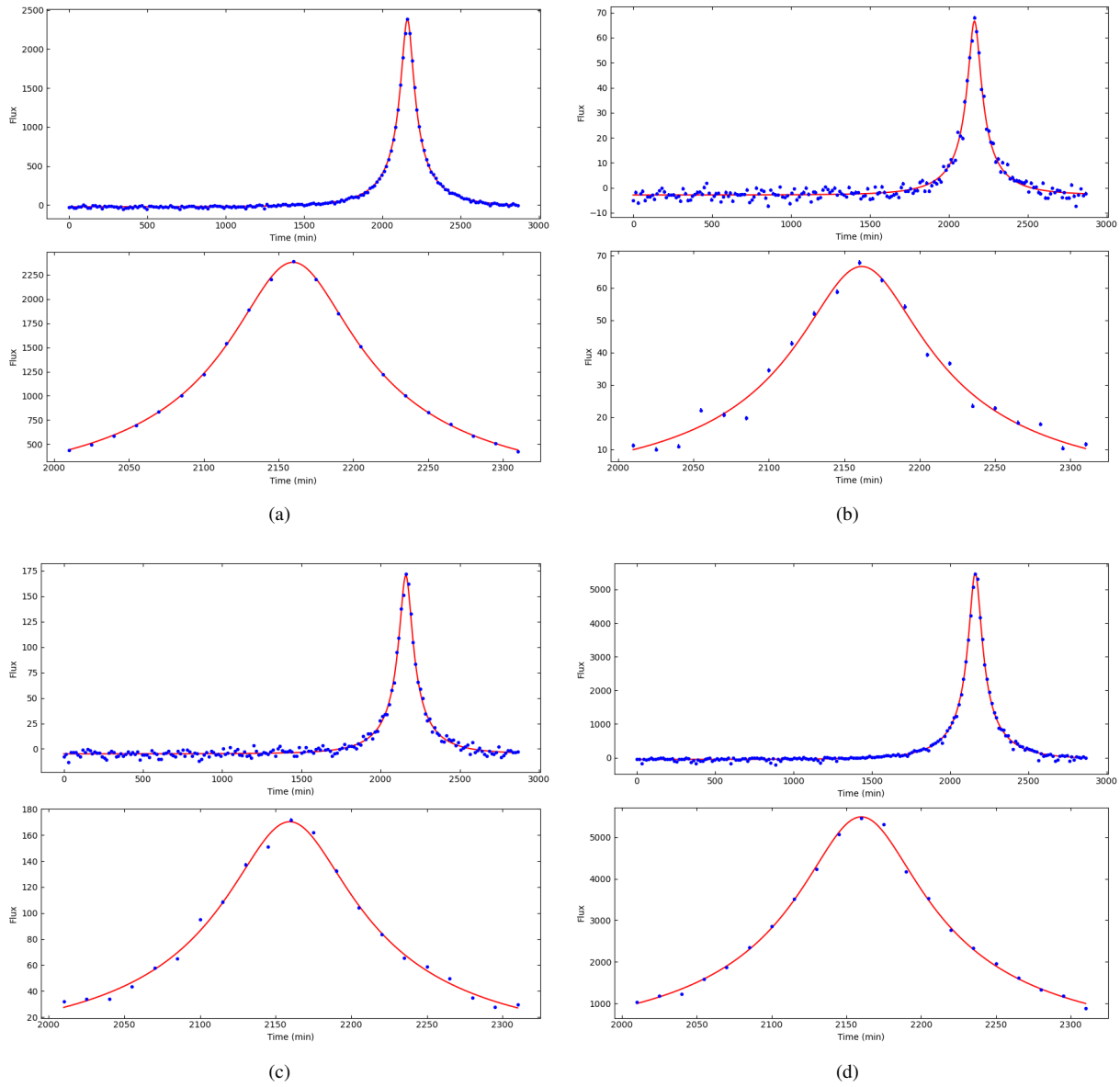

Figure 5. Complete light curves from PSF-fitting to the sets of simulated difference images shown in Fig. 4. The red lines are PSPL microlensing fits to the data.

3.5 Microlensing event detection

It is likely that most variable stars, including microlensing events, and stars with transiting exoplanets will be detected by various filtering methods from the primary direct-image photometry that will be made available from the pipeline data reduction that is being developed by the Roman Galactic Exoplanet Survey Project Infrastructure Team (RGES-PIT).

We are primarily concerned here with detection of microlensing events from the produced difference images. This might be the case for faint stars in crowded fields where the primary photometry is poor, or the source star is not present in the primary photometric catalogue.

Our approach is based on a matched filter. We begin by constructing a three-dimensional image stack, consisting of all of the difference images shifted by their integer pixel offsets of that they are approximately aligned. We then convolve the stack by a three-dimensional Gaussian kernel, which is symmetric in the two spatial directions, with a width similar to that of stellar PSF. For the third (temporal) direction we use a number of trial widths in order to detect microlensing events of differing timescales.

We then search for peaks in the resulting three dimensional array using a local-maximum filter and requiring that detected peaks are above a configurable threshold. The threshold used depends on the temporal-direction kernel width. The detected peaks identify both the approximate spatial location and the time of peak brightness of candidate events.

3.6 Photometry

For a given variable star (whether detected from the primary photometric light curves or from the difference images as discussed above), we perform PSF-fitting photometry on the difference images to measure the difference-flux of the star at each epoch. We use a grid of ten-times-over-sampled PSF's that we generated with *WebbPSF* and,

for each image, evaluate the PSF on a square grid (stamp) with sides of length $2r + 1$, with the observed image pixel scale. The evaluated PSF is centred on the assumed sub-pixel location of the star in the difference image, accounting for the dithered offset of the image relative to the reference, and the sub-pixel coordinates of the star in the reference. The flux is then,

$$F_k = \frac{\sum_{lm} P_{lm} D_{k(i+l)(j+m)} / \sigma^2_{k(i+l)(j+m)}}{\sum_{lm} P^2_{lm} / \sigma^2_{k(i+l)(j+m)}}, \tag{17}$$

with variance

$$\sigma^2_{F_k} = \frac{\sum_{lm} P^2_{lm}}{\sum_{lm} P^2_{lm} / \sigma^2_{k(i+l)(j+m)}}, \tag{18}$$

where (i, j) is the integer pixel location of the centre of the star in difference image k, and P is the grid-sampled PSF.

We optimize the coordinates of the variable star by by minimizing

$$\chi^2_F = \sum_{klm} \frac{(D_{k,lm} - F_k P_{lm})^2}{\sigma^2_{klm}}, \tag{19}$$

where (l, m) range over the difference-image stamp for a given k, and again P_{lm} is evaluated from the PSF grid taking into account the stellar coordinates and integer and sub-pixel offsets of image k from the reference.

In Fig. 4 we show an example of this process. The top row of images in the figure are of a 7 x 7 pixel region from selected images in the simulated set. Near the center of these images is a faint star (W146 = 24.69) that has had a PSPL microlensing event with $u_0 = 0.1$ injected into its flux at the time of image simulation. The microlensing event has a timescale of a few hours and would correspond to an isolated planetary-mass lens. The left- and right-most images show the field when the star is not magnified (and is not visible), and the five central images are the field at various epochs when the star is magnified (and perhaps barely visible). The central row of images are difference images (with a smaller intensity scaling) of the same parts of the field and same epochs as the top row. The magnified star is now clearly visible. The bottom row of the figure are the difference images (with the same scaling as the central row) after subtraction of the fitted PSF after optimisation of the star's coordinates from the difference images.

In Fig. 5 shows the full light curve for this star measured from the complete set of difference images. A PSPL microlensing light curve fitted to these data recovered parameters $u_0 = 0.12 \pm 0.05$, $t_0 = 2160.3 \pm 2.6$, $t_E = 330 \pm 110$ min, which can be compared to the injected parameters $u_0 = 0.1$, $t_0 = 2160$, $t_E = 400$ min.

4 IMPLEMENTATION DETAILS

The algorithms described above have been implemented in a python package that is available at https://github.com/MichaelDAlbrow/Dazzle. Along with the core package, several python scripts are provided to reproduce the results from this paper. The python code is deliberately written in a functional/procedural style.

5 SUMMARY

Summary.

ACKNOWLEDGEMENTS

The Acknowledgements section is not numbered. Here you can thank helpful colleagues, acknowledge funding agencies, telescopes and facilities used etc. Try to keep it short.

DATA AVAILABILITY

The inclusion of a Data Availability Statement is a requirement for articles published in MNRAS. Data Availability Statements provide a standardised format for readers to understand the availability of data underlying the research results described in the article. The statement may refer to original data generated in the course of the study or to third-party data analysed in the article. The statement should describe and provide means of access, where possible, by linking to the data or providing the required accession numbers for the relevant databases or DOIs.

REFERENCES

Alard C., 2000, A&AS, 144, 363
Alard C., Lupton R. H., 1998, ApJ, 503, 325
Albrow M. D., Gilliland R. L., Brown T. M., Edmonds P. D., Guhathakurta P., Sarajedini A., 2001, ApJ, 559, 1060
Albrow M. D., et al., 2009, MNRAS, 397, 2099
Anderson J., King I. R., 2000, PASP, 112, 1360
Bond I. A., et al., 2001, MNRAS, 327, 868
Bramich D. M., et al., 2013, MNRAS, 428, 2275
Bruntt H., Frandsen S., Gilliland R. L., Christensen-Dalsgaard J., Petersen J. O., Guhathakurta P., Edmonds P. D., Bono G., 2001, A&A, 371, 614
Cardelli J. A., Clayton G. C., Mathis J. S., 1989, ApJ, 345, 245
Gilliland R. L., et al., 2000, ApJ, 545, L47
Hogg D. W., Casey A. R., 2024, arXiv e-prints, p. arXiv:2403.11011
Marshall D. J., Robin A. C., Reylé C., Schultheis M., Picaud S., 2006, A&A, 453, 635
O'Donnell J. E., 1994, ApJ, 422, 158
Penny M. T., Gaudi B. S., Kerins E., Rattenbury N. J., Mao S., Robin A. C., Calchi Novati S., 2019, ApJS, 241, 3
Perrin M. D., Sivaramakrishnan A., Lajoie C.-P., Elliott E., Pueyo L., Ravindranath S., Albert L., 2014, in Oschmann Jacobus M. J., Clampin M., Fazio G. G., MacEwen H. A., eds, Society of Photo-Optical Instrumentation Engineers (SPIE) Conference Series Vol. 9143, Space Telescopes and Instrumentation 2014: Optical, Infrared, and Millimeter Wave. p. 91433X, doi:10.1117/12.2056689
Robin A. C., Reylé C., Derrière S., Picaud S., 2003, A&A, 409, 523
Sahu K. C., et al., 2006, Nature, 443, 534
Tomaney A. B., Crotts A. P. S., 1996, AJ, 112, 2872
Wilson R. F., et al., 2023, ApJS, 269, 5
Wozniak P. R., 2000, Acta Astron., 50, 421

APPENDIX A: SOME EXTRA MATERIAL

If you want to present additional material which would interrupt the flow of the main paper, it can be placed in an Appendix which appears after the list of references.

This paper has been typeset from a TEX/LATEX file prepared by the author.